BACHELOR

Optical detection of CRP binding to aptamer functionalized single gold nanorods

Creugers, Gijs

Award date:
2018

All that glitters is not gold

Except for the nanorods used in the experiments you are about to read about , they really are tiny bits of gold.

Technische Universiteit
Eindhoven
University of Technology

Optical detection of CRP binding to aptamer functionalized single gold nanorods

Gijs Creugers (0886409)

Bachelors End Project, faculty of Applied Physics
Supervisors: dr. P. Zijlstra, R.E. Armstrong
Date: 3-7-2017

Where innovation starts

Abstract

A molecular bio-sensor is an analytical device that turns a bio-molecular interaction into a measurable signal. In the case of this report this device consists of a sample of golden nanorods placed on top of a microscope. These nanorods scatter light at a certain wavelength called the plasmon wavelength. When molecules bind to a rod, its optical properties change, resulting in a shift of the plasmon wavelength. This shift can be measured and thusly used to detect molecule binding events. To make sure only the molecule of interest (in this case CRP) can bind to the rod, the surface of the rod is covered with an aptamer known to bind CRP only, while the remaining surface is filed with peg to block non specific interactions .

The goal of this report is to find how many aptamer needs to be attached to the nano-rods to obtain a optimal shift due to CRP-binding. First a simple model is used to simulate some changes of parameters and the effect of a layer of molecules around a rod, on the plasmon peak. Next to the modeling, experiments are conducted where the aptamer coverage is varied and the shift due to CRP binding is observed.

The experimental data does not show hard evidence for an optimum, but we do see that a somewhat low aptamer covered sample gives better results than a fully saturated sample.

Contents

1 Introduction

1.1 Plasmon resonances in metallic particles

The interaction of electromagnetic waves and gold nanoparticles (as well as some other noble metals) results in an collective oscillation of electrons in the conduction band. When a light wave reaches the particle the oscillating electric field moves the electrons away from the positive cores. These move back due to coulomb forces and then move the other due to oscillatory electric field. If the electric field of the incoming light beam is matching the oscillating electrons, the electrons will encounter resonance. This oscillation is known as the localized surface plasmon resonance [7]. This resonant oscillation causes large wavelength-dependent changes in absorption, scattering and electromagnetic field at the nano rod surface. A plot of this enchanced field for a nanosphere and a nanorod can be seen in *figure* 1.

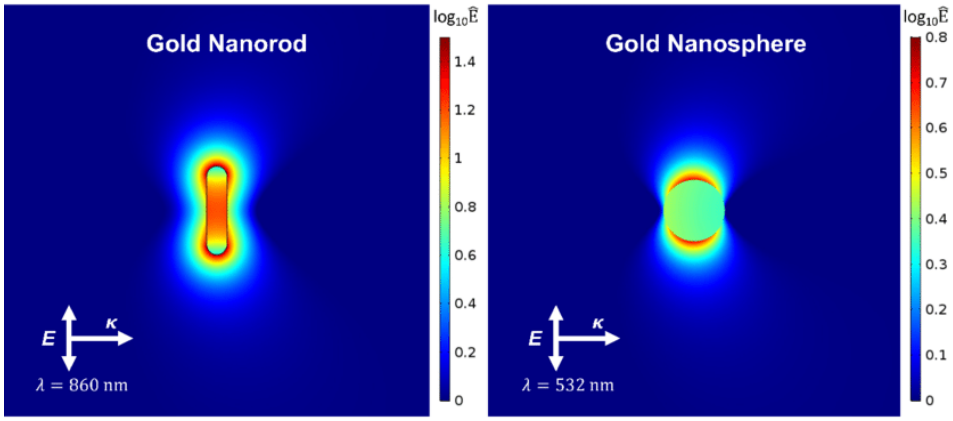

Figure 1: Plot of the relative electric field enhancement [16]

1.2 Sensing with plasmon resonances

The wavelength that results in plasmon reasonance is depending on the size, shape and environment of the particle. Because of this the binding of a molecule will lead to a plasmon shift to the red [2]. This can be used to detect particles binding to the gold nanoparticles. In our experiments we will use rods because these cause a stronger field (especially around the tips) than spheres do, and are thus more sensitive. The spectra before and after the CRP, PEG, and aptamer binds will be measured to find the corresponding shift. Also the intensity of a specific wave length can be observed during the binding process resulting in a time trace where steps in scattering intensity correspond to a binding event.

1.3 Aptamers

Aptamers are gaining interest in the development of biosensors. Aptamers are synthetic oligonucleotides that are capable of specific binding tot a variety of targets such as proteins. They can be found with high affinity and specificity, and are relative easy to manipulate and synthesize. They can be used as an alternative to antibodies and are often better in terms of cost of production, easy handling and chemical simplicity [9]. Another reason that aptamers often replace antibodies is that they are smaller in size and can target small molecules [10]. For our case this small size is especially important because this allows the molecule to bind closer to the rod where the field is high. The aptamer used has an expected Kd of 17nM and it's sequence is:

5'- CCC-CCG-CGG-GTC-GGC-TTG-CCG-TTC-CGT-TCG-GCG-CTT-CCC-C -3'

In this project aptamers capable of binding CRP are attached to gold nano rods. When the aptamers bind to the CRP the plasmon resonance frequency shifts. To obtain a big shift in frequency as many as possible proteins have to be bound to the rod. If there are only a few aptamers, they can only bind to a few proteins. On the other hand, if the aptamer coverage gets to high, we expect them to interfere with each other so that the proteins can't bind either, as is shown in *figure* 2 below. To block non specific interactions (CRP binding directly to the rod), the remaining bare surface is covered with PEG (not displayed in the figure).

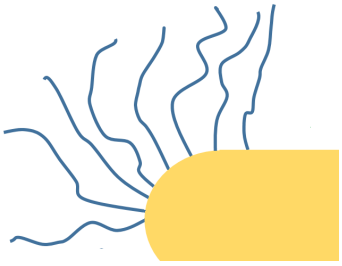

(a) Gold nanorod with high aptamer coverage.

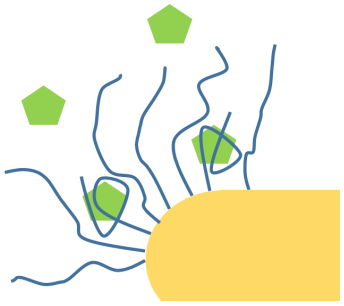

(b) crp bound to gold nanorod with high aptamer coverage.

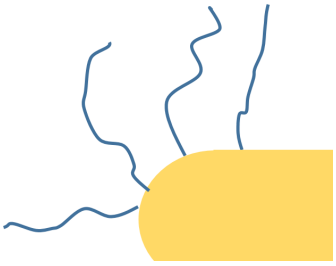

(c) gold nano rod with low aptamer coverage

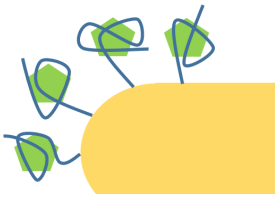

(d) crp bound to gold nanorod with low aptamer coverage

Figure 2: schematic visualization of gold nanorods (yellow) functionalized with aptamers (blue) which are binding to CRP (green) to show that simply saturating the rods with aptamer does not lead to a optimal amount of CRP binding.

1.4 Aim of this project

The aim of this bachelor's project is to use scattering total internal reflection excitation microscopy to measure the plasmon shift of C-reactive protein (CRP) binding to gold nanorods functionalized with aptamers. This will be done for various concentrations of aptamers so that the aptamer concentration resulting in the maximum plasmon shift can be obtained. It is observed that a higher aptamer coverage does not always result in a bigger shift due to CRP binding. We suppose this is can be explained because the aptamers interfere with each others way if they are packed to dense, and are therefore not able to fold around the CRP molecules.

2 theory

2.1 Mie theory

In 1908 Mie published a theory that provides an analytical solution for the scattering and absorption of light by a metal sphere [5]. This theory is derivation from Maxwell's equations with the appropriate boundary conditions [4]. Mie theory can be used to calculate the electromagnetic field inside and outside a spherical particle. If the sphere is much smaller than the wavelength of light it is possible to neglect the the variations of the electric field over the sphere's dimensions. In this case the polarizability of a small sphere is given by [12]:

$$\alpha(\omega) = 3\epsilon_0 V \frac{\epsilon(\omega) - \epsilon_m}{\epsilon(\omega) + 2\epsilon_m} \tag{1}$$

Here ϵ_m is the dielectric permittivity of the embedding medium, ϵ_0 is the vacuum permittivity, V is the volume of the particle and $\epsilon(\omega)$ is the dielectric function of gold. From this polarizability the optical cross sections of the metal spheres can be calculated.

The dielectric function of gold is experimentally determined by P. B. Johnson, and R. W. Christy [11]. These experimentally determined values are put in a Matlab function which is plotted in *figure* 3 below.

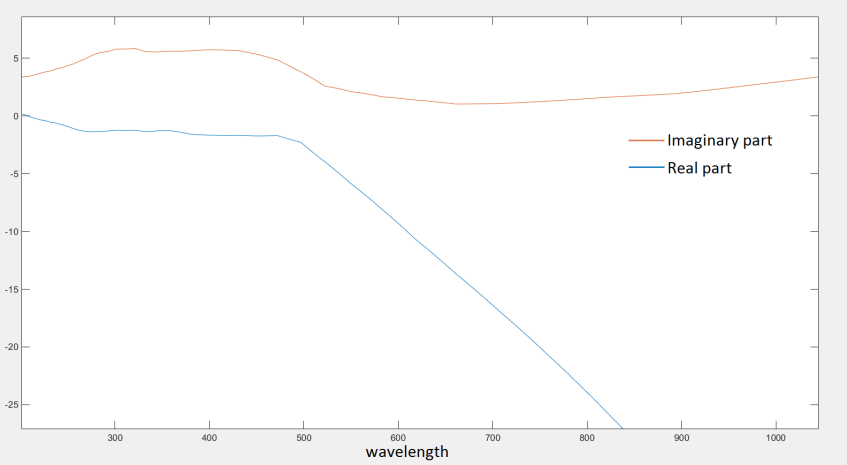

Figure 3: Real and Imaginary part of dielectric function of gold

In an experiment the polarizability is not measured directly, but the sample is irradiated with a known intensity (W/M^2), and the power (W) that is taken out of the beam is measured [12]. The ratio between power and intensity has units of area and is called the extinction cross-section. The extinction cross-section quantifies the light taken out of the beam, the scattering cross-section quantifies the light scattered by the particle. The scattering and extinction cross-section can be expressed as:

$$\sigma_{ext} = \frac{k}{\epsilon_0} \text{Im } \alpha(\omega), \text{ and} \tag{2}$$

$$\sigma_{scatt} = \frac{k^4}{6\pi\epsilon_0} |\alpha(\omega)|^2, \tag{3}$$

where k is the incoming wavevector.

2.2 Model for ellipsoidal particles: Mie-Gans theory

Mie theory is only valid for spherical particles. Therefore Mie-Gans theory is used to calculate the polarizability of elipsoids which are a good approximation for rods [6]. Mie-Gans theory is a first order approximation of Mie theory [3].
The polarizability of an elipsoid is than given by:

$$\alpha(\omega) = \epsilon_0 V \frac{\epsilon(\omega) - \epsilon_m}{\epsilon_m - L_p(\epsilon(\omega) - \epsilon_m)}, \tag{4}$$

where L_p are the depolarization factors along the principle axis of the particle with $p = (1, 2, 3)$. These factors can be expressed as:

$$L_1 = \frac{1 - e^2}{e^2}(1 + \frac{1}{2e} ln \frac{1 + e}{1 - e}), \text{and} \tag{5}$$

$$L_{2,3} = \frac{1}{2}(1 - L_1), \tag{6}$$

with $e^2 = 1 - \frac{b^2}{a^2}$ the eccentricity of the ellipsoid, so the aspect ratio is $\frac{a}{b}$ with long axis a, and short axis b. The effect of variations in aspect ratio is plotted in *figure* 4 below.

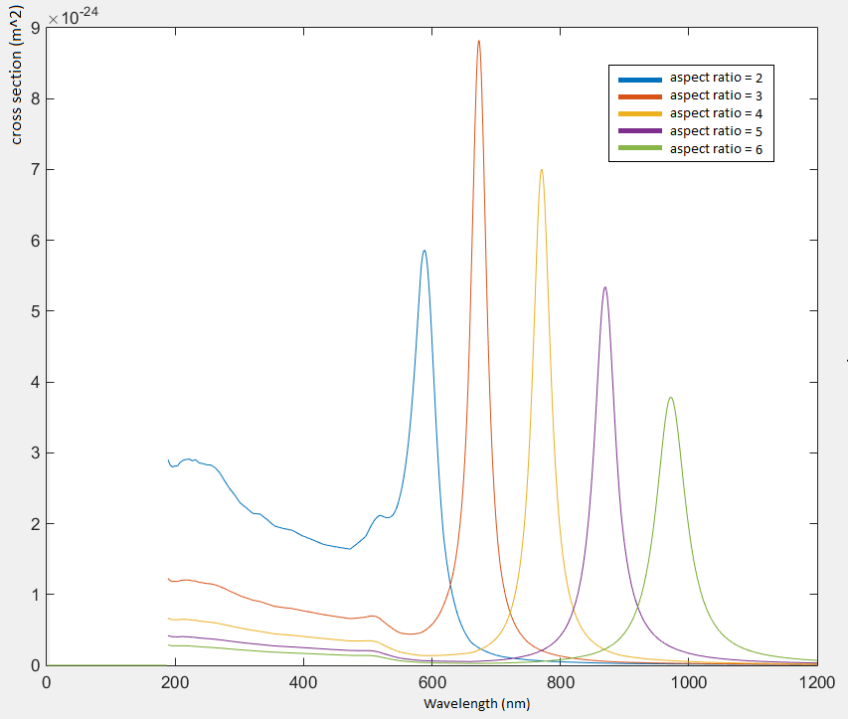

Figure 4: Scattering cross section for gold nanorod with aspect ratio ranging from 2 to 6

2.3 Ellipsoids with shell

In this thesis the effect of aptamers binding to nanorods, and CRP binding to aptamer-functionalized nanorods on the plasmon peak resonance is investigated. To be able to estimate the effect of these molecules an extended version of the Mie-Gans model above is used. For this model, the additional molecules will be approximated by a uniform layer of a certain thickness and refractive index. The polarizability of the ellipsoid with shell is now given by [2]:

$$\alpha_p = \epsilon_0 V \frac{(\epsilon_2 - \epsilon_m)(\epsilon_2 + (\epsilon(\omega) - \epsilon_2)(L_{1p} - fL_{2p}) + f\epsilon_2(\epsilon(\omega) - \epsilon_2)}{(\epsilon_2 + (\epsilon(\omega) - \epsilon_2)(L_{1p} - fL_{2p}))(\epsilon_m + (\epsilon_2 - \epsilon_m)L_{2p}) + fL_{2p}\epsilon_2(\epsilon(\omega) - \epsilon_2)}, \tag{7}$$

where ϵ_2 is the dielectric function of the shell, and L_{1p} is the depolarization factor of the core and L_{2p} is the depolarization factor of the shell, which can be calculated combining:

$$e^2_{shell} = 1 - \frac{(a_{elipsoid} + t)^2}{(b_{elipsoid} + t)^2}, \tag{8}$$

and *equation* 5 and 6 above. a and b are defined as the lengths of the short and long axis respectively, t is the thickness of the shell, and f is the volume fraction of the particle with shell by the particle: $f = \frac{(aab)}{((a+t)*(a+t)*(b+t))}$

in *figure* 5 below the scattering cross-section for elipsoids with a shell of ranging thickness is plotted.

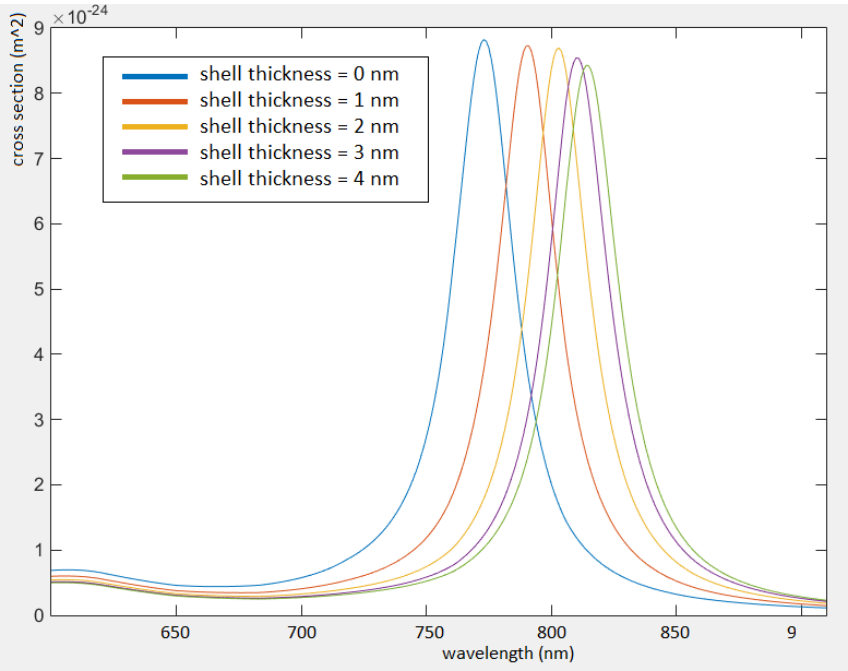

Figure 5: Scattering cross section for ellipsoids covered with protein shells of thicknesses ranging from 0 to 4nm with a refractive index of 1.47

2.4 Influence of surrounding medium on plasmon wavelength

Because we are binding aptamer, peg and CRP, which have to be stored in citrate-, PBS- and HEPES-buffer respectively, the buffers have to be switched in between measurements. These buffers have varying refractive indexes, and thus switching buffers affects the measurement. citrate is found to have a refractive index of 1.373 [13], PBS 1.334 [14], and HEPES 1.339 [14]. The plasmon of a ellipsoid of aspect ratio 3.5 is plotted for all the three buffers in *figure* 6. It can be seen that according to the model switching from citrate to PBS results in a 6nm blue-shift, and switching from PBS to HEPES results in a 1nm blue-shift.

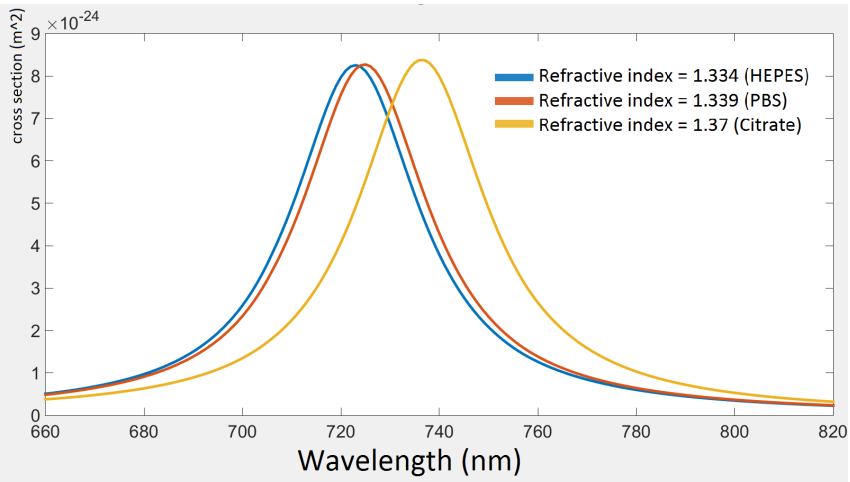

Figure 6: Scattering cross section for ellipsoids of aspect ratio 3.5 surrounded by varying refractive indexes

2.5 Remarks on model

The model described in the previous paragraphs is a neat tool for quick calculations on plasmon resonance frequencies. Nevertheless there are a few aspects that can cause a deviation between the model and reality. First of all the rods are approximated as ellipsoids, this causes a deviation in volume and the curvature of the tips is different which affects the plasmon peak and shift.
Next to that, in reality the rods are attached to the glass surface. This will cause a small red shift, and causes a less surface available for binding molecules. Also it is not exactly know how the particles bind and if they indeed form a evenly shell. Another point of discussion is the thickness of the layer. For a small molecule like peg the thickness might be well approximated by the length of the molecule, but molecules that are long compared to their persistence length, such as aptamers, will have an effective length shorter than the actual length of the molecule. Although these deviations from reality will cause the plasmon peak positions and scattering cross-section to differ slightly, we believe that it is still useful for estimating the outcome of the experiments.

3 Methods

3.1 Single molecule dark-field microscopy

A fibre-coupled light source radiates a light beam under an angle to create a light beam exiting the objective with an angle larger than the critical angle. Most of this light will be totally internally reflected from the glass-water interface. An evanescent field is created at the interface of glass with the flow by which the gold rods are exited. The light scattered by the rods is collected by the CCD camera positioned under the sample. In our experiments the light source is either an infrared laser or a white light source, depending on the type of measurement as explained in the paragraphs below. The microscope is equipped with a water-oil immersion objective. This means that the gap between the objective is filled by a droplet of water, and the prism is attached to the sample by a droplet of oil. The prism is used to decrease the angle of incidence of the beam in the air. A typical image obtained with this setup is shown in *figure* 7b.

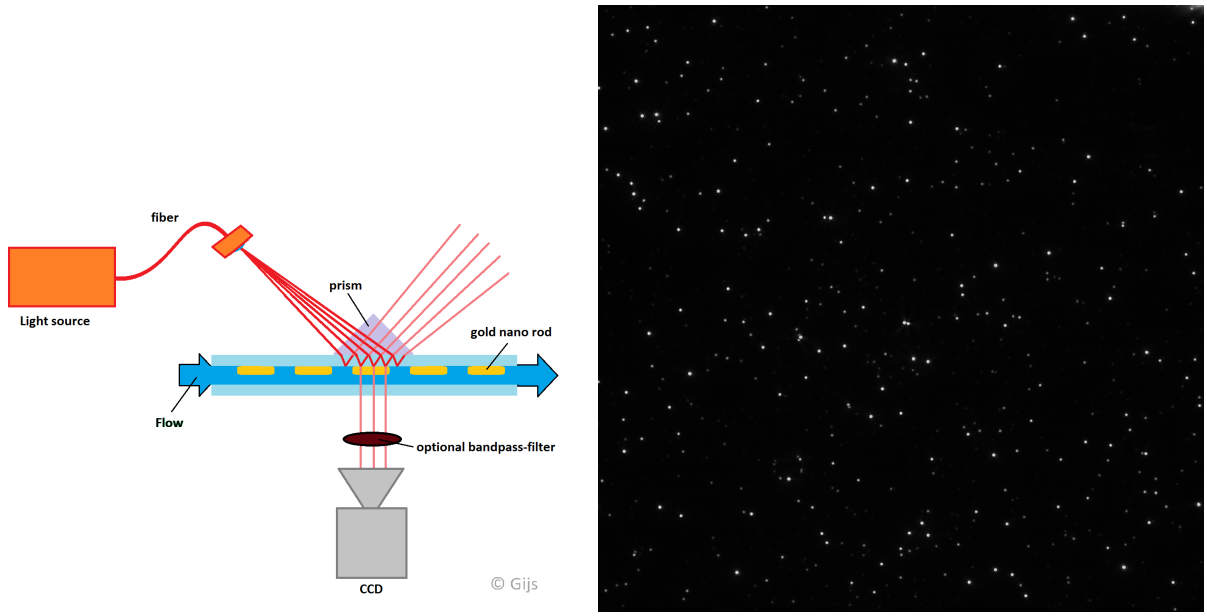

(a) Experimental setup

(b) A typical field of view

Figure 7

3.2 Hyper-spectral measurement

The spectra of nanorods are determined with a hyper-spectral measurement. This means that a series of bandpass filters is inserted in the white-light path of the microscope while for every filter a snapshot is taken. The intensity for every wavelength is determined by fitting a Lorentzian through the obtained data points. Unlike regular spectroscopy, that takes the average of the sample, with this technique the spectra for many individual nanorods can be obtained at once [1].

3.3 Error estimation of hyperspectral measurements

To estimate the error in a hyperspectal measurement, multiple measurements of the same sample have been compared. In *figure* 8 the distribution of differences between measurement 1 and measurement 2 per particle have been plotted. In the ideal case this graph would look like a narrow spike at zero, meaning both the measurements are identical. As can be seen in the figure, at single particle level the difference in measurements can be up to 8nm, thanks to statistics the deviation in the average over the whole sample is much smaller (when the number of particles is high enough).

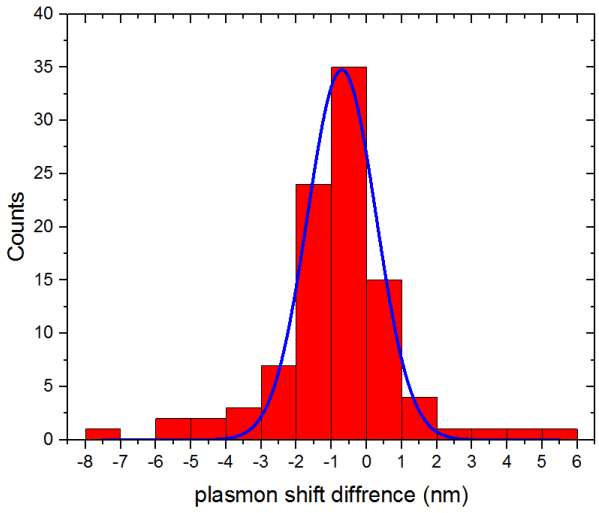

Figure 8: Distribution of difference in plasmon peak position (per particle) for two measurements of the same sample

3.4 Kinetic measurement

It takes a few minutes to obtain a hyperspectral data, so this can only be done for an stationary sample (before and after adding molecules to the rods). To be able to observe the sample while adding a certain analyte, time-trace measurements are used. In this case the 780nm SLD is used to iluminate the sample. Because this is a very specific wave length the scattered intensity is dependent of the position of the peak relative to the laser wavelength. If the laser wavelength is on the right side of the peak, a red-shift will result in the intensity going up, while if the laser-wavelength is on the left, the intensity will go down. It can even go up and than down in the case that is starts on the right and ends up on the left. This is displayed in *figure* 9.

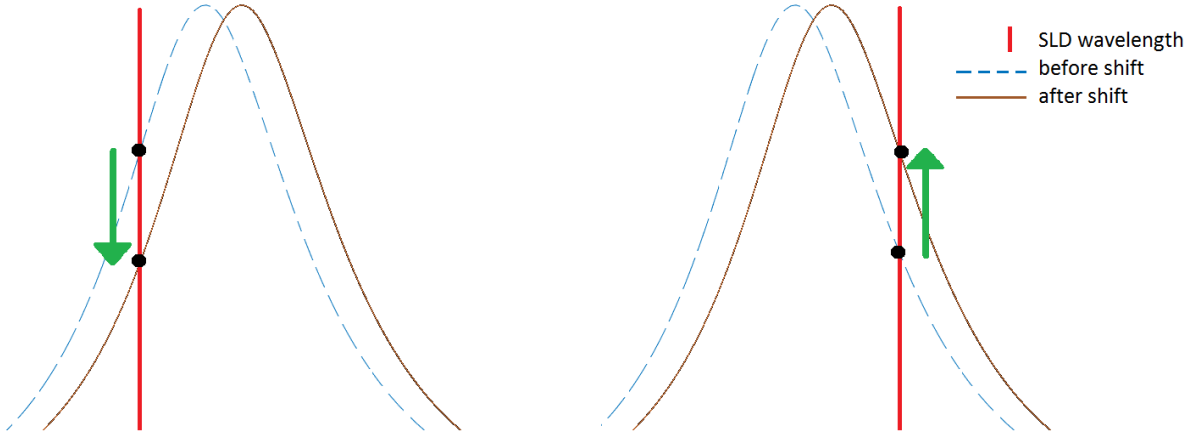

Figure 9: If sld wavelengt is on left hand side, the scattered intensity will decrease for a redshift. If the sld wavelength is on the right hand side, the scattered intensity will increase for a redshift

3.5 Sample preparation

In this project golden nanorods with a diameter of 22nm, length of 70nm and plasmon wavelength of 750nm fabricated by NanoSeedz are used. These rods are spin-coated on a glass cover slip by my supervisor. Both the PEG and aptamer have a thiol at the end to bind to the nanorod. The coverslips with gold nanorods are mounted in a flowcell. This flowcell setup allows us to measure while changing the solution around the sample without loosing the positions of the particles.
Our experiments are started with a citrate buffer in the flowcell so that the aptamer is able to bind to

the rod. In these experiments a solution with 500μM aptamer is used. The exposure time of the rods to the solution containing aptamer is varied so that variating aptamer coverages on the rods are obtained . After the exposure time of the aptamer expired the citrate buffer is flowed back in. Thereafter PBS-buffer is flowed in and PEG is added long enough to cover the remaining bare surface of the rod. Now the rod is fully covered with aptamer+PEG the buffer is switched to the CRP-binding-buffer and the CRP is added to the flowcell.
The PEG, aptamer, and CRP is added during a timetrace measurement.Hyperspectral images are obtained before and after the binding of PEG, aptamer, and CRP.

4 Results and Discussion

The first data that are obtained are the plasmon peaks of the bare rods by hyperspectral imaging. Processing these images with Matlab results in a graph for every particle showing the data points corresponding to the 18 bandpass filters and a Lorentzian fit trough these data point. A graph like this can be seen in *figure* 10.

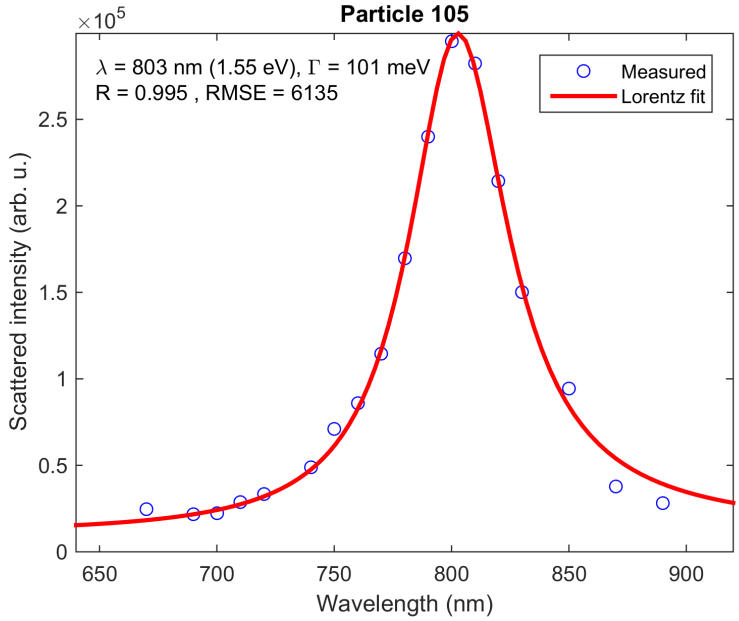

Figure 10: Example of a plasmon peak of a particle

Due to variation in the shape, more specific the aspect ratio, of the particles, it is seen that the plasmon peaks are not the same for all the particles. It is observed that these peaks are gausian distributed. This is what we would expected form the model as explained in *paragraph 2.2.* An example of such a distribution of plasmonpeaks is shown in *figure* 11.

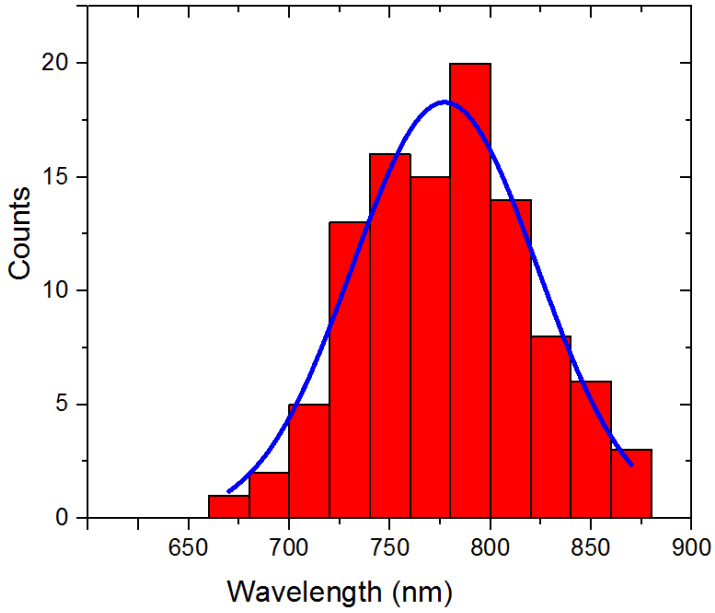

Figure 11: distribution of plasmon peaks

4.1 Aptamer binding

Now that the spectra of the bare rods are known, the aptamer is flowed into the sample while doing a time-trace measurement. This measurement provides graphs like the two shown in *figure* 12. In these graphs a clear shift is seen when the aptamer hits the flowcell. Also it can be seen that a shorter exposure time results in less plasmon shift which is in agreement with what would be be expected.

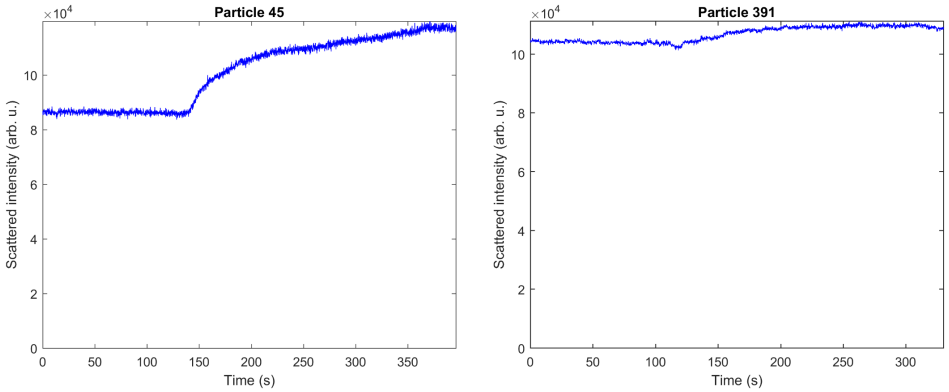

Figure 12: timetrace signal for a aptamer exposure time of 120 sec (left) versus a exposure time of 12 sec (right)

After this another hyperspectral-measurement is done, so that the shift due to the aptamer binding can be calculated. A before- and after-aptamer plasmon peak is shown in *figure* 13 below.

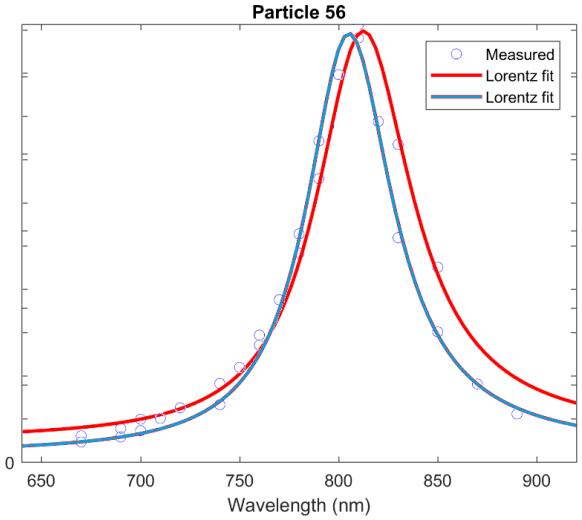

Figure 13: example of a plasmonpeak before and after binding to aptamer

4.2 PEG binding

Before the PEG can be added the citrate-buffer has to be replaced by a PBS-buffer. The refractive index of PBS-buffer deviates from the refractive index of the citrate-buffer. So changing the buffer will lead to plasmon-shift, as can also be seen in the modeling in *paragraph 2.4*. Because of this, the after-aptamer data can not just be used as before-PEG data, so a new hyperspectral measurement has to be done.

In *figure* 14 below a timetrace for PEG binding to a aptamer-saturated sample versus a control sample without aptamer is shown.

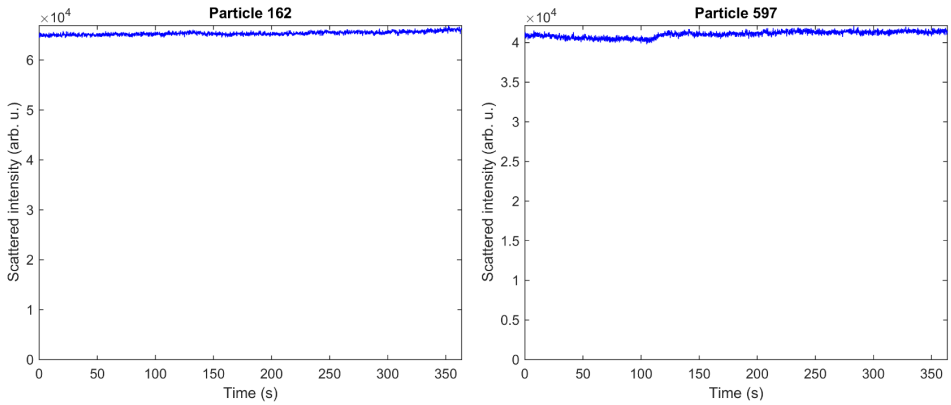

Figure 14: timetrace signal of PEG binding to a high aptamer covered sample (left) versus a low aptamer covered sample (right)

4.3 CRP binding

After the rods are coated with a combination of aptamer and PEG the 'CRP-biosensor' is ready for use. Again a before- and after-hyperspectral measurement is done, and during the process a timetrace is recorded. An example of this is shown in *figure* 15.

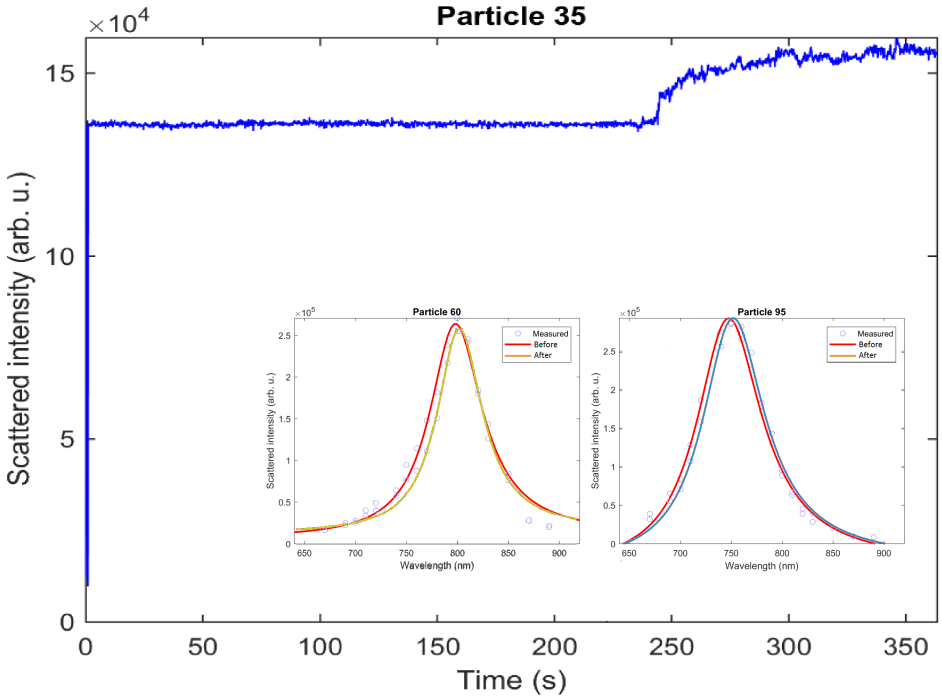

Figure 15: a) timetrace signal for CRP binding to a particle b)+c) example of plasmon shift due to CRP binding

4.4 Control measurements

For a reliable biosensor specificity is important. If the sensor is not specific enough non-specific binding will cause false positives. To investigate non specific binding a set of control measurements is executed. First CRP is added to a sample of bare rods to verify the presence of non specific binding. In *figure* 16a below the distribution of plasmon shifts for this sample is shown, and it can be seen that the average shift is 4.4 nm to the red and thusly we can conclude that the CRP is directly binding to the rods as anticipated.

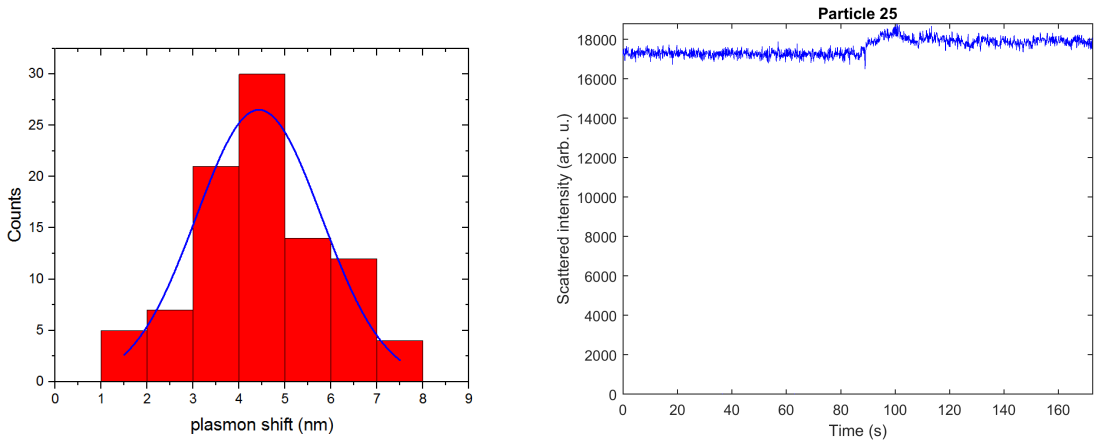

(a) distribution of plasmonshifts for control measurement of CRP binding to bare rods (b) example timetrace for crp binding to bare nanorods

Figure 16

To eliminate the binding of CRP directly to the rods the bare surface is covered with a small peg molecule . To test if this indeed blocks the non specific binding of CRP a second control measurement is executed. This time a sample of bare rods wil be fully coated in peg (so no aptamers) after which CRP is flowed in. The distribution of shifts for this measurement is shown in *figure* 17a. In contrast to what is expected a not-insignificant red-shift of 3.7 nm is observed, the cause and/or concequence of this unexpected shift will be discussed in *paragraph 5*.

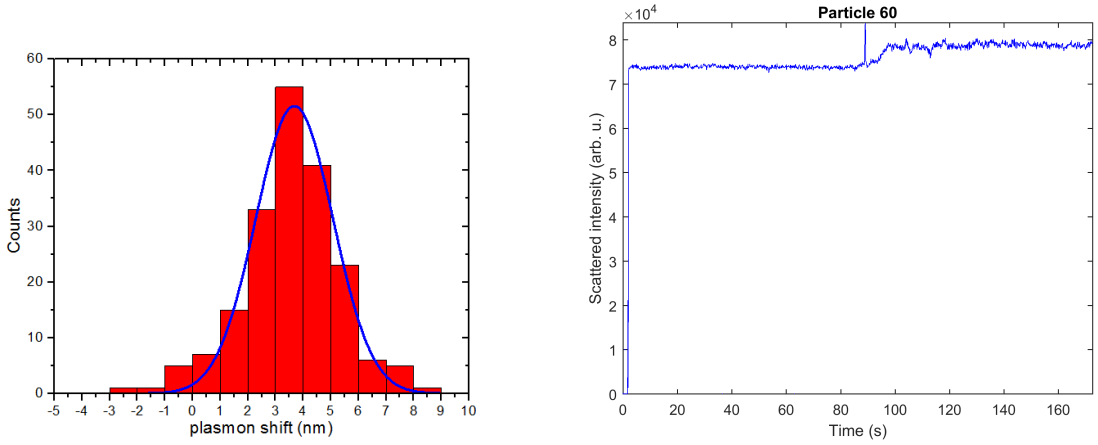

(a) distribution of plasmonshifts for control measurement of CRP binding to PEG covered rods (b) example timetrace for crp binding to PEG covered nanorods

Figure 17

4.5 CRP shift versus aptamer coverage

The goal of this project is to find a relation between the number of aptamers on a gold nanorod and the plasmonshift resulting from adding CRP. Since it is not possible to count the exact number of aptamers, this is done in the form of a plot of aptamer shift versus CRP shift as shown in *figure* 18. The spread of these data points together with the low number of data points makes it hard to fit it with a function, But the hypothesis of an optimum for a relative low aptamer coverage could be right.

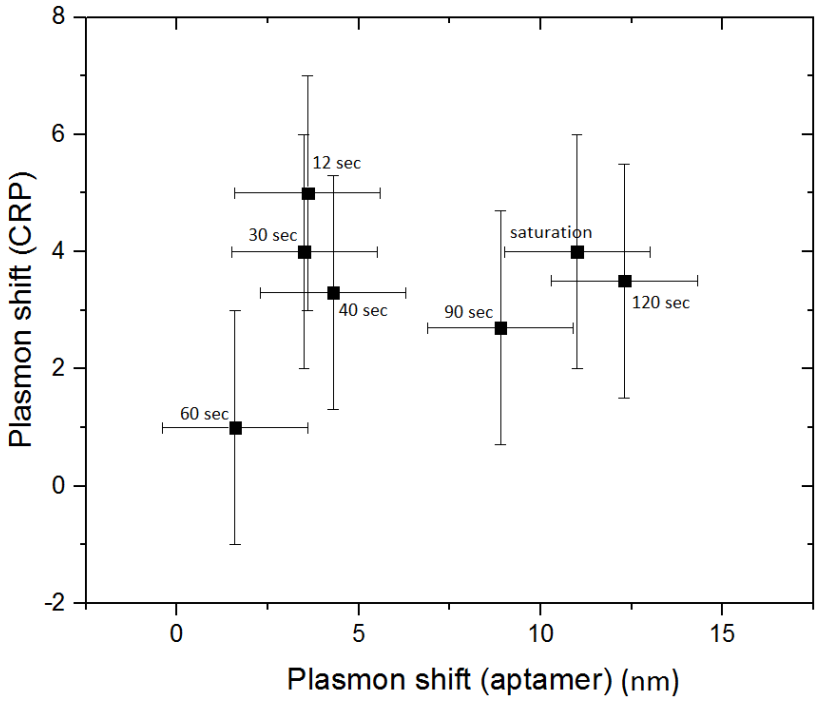

Figure 18: plasmon shift due to aptamer versus shift due to CRP. Variations in shifts are obtained by varying the eposure time of the sample to aptamer (as labled in the graph)

5 Discussion and Conclusion

In this thesis plasmon shifts caused by CRP binding to aptamer functionalized golden nanorods are measured. This is done for varying aptamer coverages so that the coverage resulting in the biggest shift can be determained. Unfortunately the spread in the data was to big to observe a clear correlation, and thusly an optimal aptamer coverage was not found. This is probably caused by a combination of errors. First, there is an error of a few nanometers in the hyperspectral measurement, as we saw in *paragraph 4.6*. This error affects the aptamer shift, as well as the CRP shift, and is therefore definetly not insignificant.This error is minimized by increasing the number of nanorods used in the analysis.
An other remarkable observation is that the correlation between the exposure time and aptamer shift is not clearly present. This might partly be caused by a big error in the exposure time, because it is hard to determine when exactly the aptamers reach the flowcell, and when they are flushed away by the buffer (I would estimate this error around 3-5 seconds). However the lack of correlation between the exposure time and aptamer shift is bigger than can be explained with only a error in the timing. This might be an indication that the whole system is less predictable than on beforehand assumed.
It is expected that no PEG will bind for a sample saturated with aptamer and thusly will not shift, while samples with lower aptamer coverages will lead to more bare surface for the PEG to bind and thusly a bigger shift. This is in accordance with the observations in *paragraph 4.2*
However the control sample (*paragraph 4.4*) consists of fully peg covered rods, it still shows a shift when adding CRP unlike expected. This could mean that the rods are not fully covered with peg and still allow non specific binding, or the rods are fully covered with peg, but the CRP binds to peg, or I did something wrong during the experiment. Unfortunately due to time constraints we could not eliminate the third reason by repeating the experiment. A good way to improve this research would be by obtaining more data points so that the correlation between aptamer shift and CRP shift becomes more clear.

6 Literature

[1] M. A. Beuwer, M. W. J. Prins, and P. Zijlstra,"Stochastic Protein Interactions Monitored by Hundreds of Single-Molecule Plasmonic Biosensors",Nano Lett., 2015, 15 (5), pp 3507–3511, 2015.

[2] Mingzhao, Philippe Guyot-Sionnest,"Synthesis and Optical Characterization of Au/Ag Core/Shell Nanorods",J. Phys. Chem. B, 2004, 108 (19), pp 5882–5888, 2004.

[3] A. Akouibaa, M. Benhamou, A. Derouiche,"Simulation of the Optical Properties of Gold Nanorods : Comparison to Experiment", ijarcsse Volume 3, Issue 9, September 2013.

[4] C. Kittel,"introduction to solid state physics".Wiley, New-York, 1956.

[5] G. Mie,"Beitrage zur optik truber medien, speziell kolloidaler metallosungen," Ann. Phys., vol. 25, pp. 377-445, 1908.

[6] R. Gans,"Form of ultramicroscopic particles of silver", Ann. Phys., vol. 47, pp 270-284, 1915.

[7] S. Unser, I. Bruzas, J. He, L.Sagle,"Localized surface plasmon resonance biosensing current challenges and approaches", sensors 2015, 15, 15684-15716, 2015.

[8] P.K. Jain, K.S. Lee, I.H. El-Sayed,"calculated absorption and scattering properties of gold nanoparticles of diffrent size, shape and composition: applications in biological imaging and biomedicine", J. Phys. Chem. B, 110, 7238-7248, 2006.

[9] S. Song, L. Wang, J. Li, C. Fan, J. Zhao, "Aptamer-based biosensors", elsevier vol.27, issue 2, 2008.

[10] R. E. Wang, Y.Zhang, J. Cai, W. Cai, T. Gao,"Aptamer-based fluorescent biosensors", Curr Med Chem.1; 18(27): 4175–4184, 2011.

[11] P. B. Johnson, and R. W. Christy, “Optical constants of noble metals,” Phys. Rev. 4370–4379, 1972.

[12] P. Zijlstra, M. Orrit, A.F. Koenderink,"Metal nanoparticles for microscopy and spectroscopy", Nanoparticles : Workhorses of Nanoscience, 2014.

[13] https://hamptonresearch.com/product_detail.aspx?cid=4&sid=70&pid=135

[14] http://www.pnas.org/content/suppl/2012/10/03/1208440109.DCSupplemental/pnas.1208440109_SI.pdf

[15] https://gregemmerich.files.wordpress.com/2012/11/lspr.jpg?w=400&h=168&resize=400%2C168

[16] https://www.researchgate.net/publication/311742948_A_computational_analysis_of_nanoparticle-me